ISPRS Journal of Photogrammetry and Remote Sensing 64 (2009) 1–16

Contents lists available at ScienceDirect

ISPRS Journal of Photogrammetry and Remote Sensing

journal homepage: www.elsevier.com/locate/isprsjprs

Full-waveform topographic lidar: State-of-the-art

Clément Mallet *, Frédéric Bretar

Laboratoire MATIS - Institut Géographique National, 2-4 Avenue Pasteur 94165 Saint-Mandé Cedex, France

ARTICLE INFO

Article history:
Received 15 May 2007
Received in revised form
12 September 2008
Accepted 12 September 2008
Available online 29 October 2008

Keywords:
Lidar systems
Full-waveform data
Literature survey
Waveform analysis
Signal processing

ABSTRACT

Airborne laser scanning (ALS) is an active remote sensing technique providing range data as 3D point clouds. This paper aims at presenting a survey of the literature related to such techniques, with emphasis on the new sensors called full-waveform lidar systems. Indeed, an emitted laser pulse interacts with complex natural and man-made objects leading to a temporal distortion of the returned energy profile. The new technology of full-waveform laser scanning systems permits one to digitize the complete waveform of each backscattered pulse. Full-waveform lidar data give more control to an end user in the interpretation process of the physical measurement and provide additional information about the structure and the physical backscattering characteristics of the illuminated surfaces. In this paper, the theoretical principles of full-waveform airborne laser scanning are first described. Afterwards, a review of the main sensors as well as signal processing techniques are presented. We then discuss the interpretation of full-waveform measures with special interest on vegetated and urban areas.

Contents

* Corresponding author. Tel.: +33 1 43 98 80 00x7566; fax: +33 1 43 98 85 81.
E-mail addresses: clement.mallet@ign.fr (C. Mallet), frederic.bretar@ign.fr (F. Bretar).
URLs: http://recherche.ign.fr/labos/matis (C. Mallet), http://recherche.ign.fr/labos/matis (F. Bretar).

0924-2716/$ – see front matter
doi:10.1016/j.isprsjprs.2008.09.007

1. Introduction

Airborne laser scanning (ALS) is an active remote sensing technique providing direct range measurements between the laser scanner and the Earth's topography. Such distance measurements are mapped into 3D point clouds. The altimetric accuracy of a topographic lidar measurement is high (<0.1 m). Depending on the geometry of illuminated surfaces, several backscattered echoes can be recorded for a single pulse emission. This is particularly interesting in forested areas, since lidar systems can measure both the canopy height and the terrain elevation underneath at once, contrary to photogrammetric techniques. Moreover, lidar data are known to be useful in many specific applications such as 3D city modeling, bridge and power line detection or Digital Terrain Model generation.

Airborne lidar data only give a basic geometric representation of a scene. Consequently, many authors have developed new automatic mapping algorithms for point classification (Filin, 2002; Sithole, 2005), urban reconstruction (Haala and Brenner, 1999; Rottensteiner and Briese, 2002) and forest assessment (Hyyppä et al., 2004). Most of them are only based on the point cloud geometry and sometimes on the intensity (Hug and Wehr, 1997).

Since 2004, new ALS commercial systems called **full-waveform** lidar have appeared with the ability to record the complete waveform of the backscattered signal echo. Thus, in addition to range measurements, further physical properties of objects included in the diffraction cone[1] may be derived with an analysis of the backscattered waveforms.

This article presents a state-of-the-art on full-waveform lidar systems as well as related processing techniques. First, we describe the physical principles of lidar systems as well as the theoretical contribution of full-waveform lidar. The second part of the article is a taxonomy of both bathymetric, experimental, and commercial full-waveform systems. We especially focus on the first main systems, developed by NASA and carried by satellite platforms. Then, full-waveform data processing methods are presented. Studies on the relationship between geometric and radiometric surface parameters and pulse shapes are discussed. Eventually, we conclude with a detailed description of full-waveform lidar data applications both on forested areas – including parameter estimation and modeling – and urban areas.

[1] The term "diffraction cone" will be used in this article in preference to "laser footprint". We would like to emphasis the fact that the laser beam reaches several objects at different heights whereas the term "laser footprint" is when the beam reaches the ground (2D consideration).

2. Topographic laser scanning systems

2.1. Presentation of airborne and spatial systems

2.1.1. Introduction

A topographic lidar device is a laser rangefinder delivering a reliable, accurate but irregular representation of terrestrial landscapes through georeferenced 3D point clouds (Baltsavias, 1999b). The first active sensors carried by airborne or satellite platforms were designed at the beginning of the 1970s. They provided 1D profiles along the sensor track (nadir view) by sequences of single pulses. Modern sensors acquire many parallel strips of 150–600 m swath width, which may overlap, due to a specific scan pattern. Such technology provides denser point clouds with a more regular distribution on the Earth's surface: the point density can reach more than 100 pts/m^2 in some specific applications, *e.g.*, river dike monitoring.

Topographic lidar is now fully operational for many specific applications such as metrology (Fidera et al., 2004), forest parameters estimation (Andersen et al., 2005), target or power line detection (Sithole and Vosselman, 2006), corridor, coastal (Irish and Lillycrop, 1999) or opencast mapping.

2.1.2. Physical principles

Both pulsed and continuous wave lasers are being used. Pulsed systems measure the round-trip time of a short light pulse from the laser to the target and back to the receiver. Continuous wave systems carry out ranging by measuring the phase difference between the transmitted and received signal. This state-of-the-art focuses on pulsed systems.

ALS physical principle consists in the emission of laser pulses from an airborne platform at a high repetition frequency (PRF). The two-way runtime of the backscattered signal from the sensor to the Earth surface is measured: it enables range estimation from the lidar system to the landscape (Baltsavias, 1999b).

Depending on the wavelength, the emitted electromagnetic wave interacts with atmospheric particles (absorption or scattering, known to have negligible influence if rain is excluded), but mainly with illuminated natural or man-made objects belonging to the Earth surface.

The PRF depends on the acquisition mode (see part 2.2.3) and on the flying altitude. A pulse release is done when the previous pulse recording is effective (even if, in fact, the PRF is constant). However, the latest systems have even the ability to fire a second laser pulse before the recording of the previous pulse (Roth and Thompson, 2008).

3D point cloud is obtained by direct georeferencing processes: a system using both GPS (differential measurements with a ground

station located near the survey area) and inertial measurements (IMU) is used to optimally calculate supporting vector attitudes and the absolute orientation of the laser sensor (Heipke et al., 2002).

Basic airborne lidar systems consist of a laser transmitter and a receiver (rangefinder unit which receives the reflected pulses and measures the distance), a mechanical scanner, a hybrid positioning system, a storage media, and an operating system for signal digitization and on-line data acquisition. This unit monitors and synchronizes measurements, and processes data in real-time to extract georeferenced points (Baltsavias, 1999a; Thiel and Wehr, 2004).

2.1.3. Lidar measurement formulas

The standard lidar equation is derived from the radar equation. It describes the measurement process by taking the detector and target characteristics into account. It also relates the power of transmitted and return signals (Jelalian, 1992). More explicit formulas have been proposed to model real world constraints (Der et al., 1997; Carlsson et al., 2001). Nevertheless, they are only valid for single sources or for flat surfaces. In case of targets that are distributed in space, the reflected signal is the superposition of echoes at different distances.

It can be expressed as an integral:

$$P_r(t) = \frac{D^2}{4\pi\ \lambda^2} \int_0^H \frac{\eta_{\text{sys}}\ \eta_{\text{atm}}}{R^4} P_t\left(t - \frac{2R}{v_g}\right) \sigma(R)\mathrm{d}R \tag{1}$$

where t is the time, D the aperture diameter of the receiver optics, P_r the received power, P_t the emitted power, λ the wavelength, H the flying height, R the distance from the system to the target, η_{atm} and η_{sys} respectively the atmospheric and system transmission factors, v_g the group velocity of the laser pulse, and $\sigma(R)\mathrm{d}R$ the apparent effective differential cross-section (Wagner et al., 2006). The cross-section is called "apparent" since an object reflecting the signal at a given distance can occlude an object further away.

The power of the received signal can also be considered as the sum of the contribution of N targets with their own characteristics:

$$P_r(t) = \sum_{i=1}^{N} P_{r,i}(t) * \eta_{\text{sys}}(t) * \eta_{\text{atm}}(t) \tag{2}$$

where $P_{r,i}(t)$ is the echo of the ith object expressed as:

$$P_{r,i}(t) = \frac{D^2}{4\pi\ \lambda^2} \int_{R_i-\Delta R}^{R_i+\Delta R} \frac{1}{R^4} P_t\left(t - \frac{2R}{v_g}\right) \sigma_i(R)\mathrm{d}R \tag{3}$$

where R_i is the mean distance, $[R_i - \Delta R, R_i + \Delta R]$ the spatial spread and $\sigma_i(R)$ the effective differential backscattering cross-section. The reflected signal can be seen as the convolution between the transmitted pulse and the effective differential cross-section. As a consequence, when $\Delta R \ll R$, we have:

$$P_{r,i}(t) \approx \frac{D^2}{4\pi\ \lambda^2\ R_i^4} P_t(t) * \sigma_i'(t) \tag{4}$$

where $\sigma_i'(t)$ is the apparent cross-section of illuminated areas within each range interval. The power of the received signal can finally be expressed as:

$$P_r(t) = \sum_{i=1}^{N} \frac{D^2}{4\pi\ \lambda^2\ R_i^4} \underbrace{P_t(t) * \eta_{\text{sys}}(t)}_{\text{system contribution}} * \underbrace{\eta_{\text{atm}}(t) * \sigma_i'(t)}_{\text{environment contribution}} . \tag{5}$$

2.2. Topographic lidar technology

2.2.1. Multiple pulse systems

The first commercially available airborne laser scanners provided only one backscattered echo per emitted pulse. The recording of a single echo is sufficient if there is only one target within the diffraction cone. However, even for small laser footprints (0.2–2 m), there may be many objects within the travel path of the laser pulse: individual scattering contributions are generated for each encountered object. **Multi-echo** or **multiple pulse** laser scanning systems are designed to record more than one echo. They typically collect first and last pulses. Some are able to discriminate up to six individual returns from a single pulse (Thiel and Wehr, 2004). The two first echoes contain about 90% of the total reflected signal power. Real-time detection of more than five pulses requires thus the detection of low intensity signal within noise.

Fig. 1 shows a comparison between first pulse and last pulse in a urban area. Two Digital Elevation Models have been generated from first pulse and last pulse point clouds. Thus, the height difference has been computed. Multiple reflections occur on vegetated areas. When the vegetation is not very dense, it is often assumed that the first echo belongs to the canopy top and the last pulse to the ground. In reality this is not always the case. It can only be checked with 3D display tools. In a particular viewing angle, when the laser beam hits a building edge, two echoes can be generated. The first pulse corresponds to the roof while the second one to the ground.

2.2.2. Geometric quality of laser scanning

Laser altimetry is a technique known to provide elevation data with reliability and high altimetric accuracy (<0.1 m) as well as a good planimetric accuracy (<0.4 cm) even under forested areas (Ahokas et al., 2003). Compared with multi-stereo high-resolution photogrammetric products, lidar points are certainly more accurate but less dense. Irregular spatial sampling is one of the main problem, as the density of points rarely exceeds 25 pts/m^2 for particular applications. The lack of information from commercial firms on real-time 3D point calculation methods makes it difficult to know the local measurement errors within the point clouds. Nevertheless, many errors alter the range measurement. Among the general error budget, systematic errors can be calibrated (bias in measuring the mirror angle, hardware problems in synchronizing and integrating measurements, incorrect point detection during real-time analysis, GPS/IMU co-ordinations etc) whereas random ones cannot (IMU temporal drift, variations in the signal to noise ratio of the return signal, electronics accuracy and surface reflectivity variations within the diffraction spot).

The errors on lidar measurements have been studied in detail by many authors (Schenk, 2001). A more detailed description of determining the position of the aircraft can be found in Bretar (2006) whereas Huising and Pereira (1998) list the main sources of errors in the laser measurement for various detectors.

2.2.3. Pulse detection methods

For multi-echo systems, pulse detection is performed in real-time on the backscattered signal. The hardware system detector turns a continuous waveform to several time-stamped pulses, giving the position of individual targets. Many peak detection methods exist, but lidar manufacturers do not provide any information about the method implemented in their hardware systems. The number and the timing of the recorded pulses are critically dependent on the detection method (Wagner et al., 2004; Jutzi and Stilla, 2005a). Fig. 2 presents an example of wrong pulse detection with the threshold method. An erroneous detection (*e.g.*, weak echoes missed) could lead to a misinterpretation of the

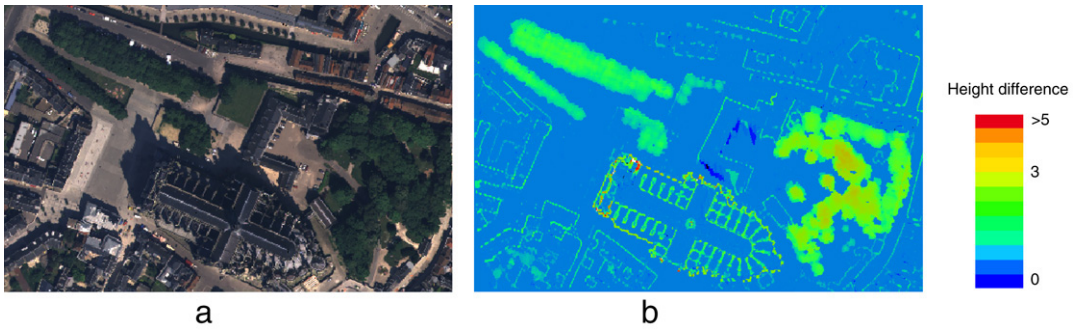

Fig. 1. First pulse and last pulse height comparison. Vegetated areas and building edges are clearly visible. (a) Orthophotography on the city of Amiens, France (0.25 m resolution ©IGN). (b) Difference between first and last pulse Digital Elevation Models.

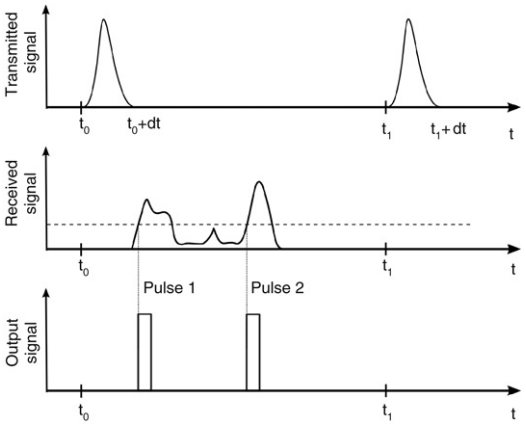

Fig. 2. Simplified pulse emission (*above*) and the corresponding received signal (*middle*). Two significant peaks are detected with the threshold method (*middle and bottom*). Two echoes will be generated for this pulse instead of four.

survey area, whereas a shift between the real-time detected pulse position and the real location leads to an inaccurate position of the object (more than 0.3 m in some cases). Moreover, in presence of low ground vegetation in woodlands or street items in urban areas, the detection method would not be able to find two echoes if the range between two targets is less than 1.5 m. Lidar waveform processing permits to cope with most of these issues.

2.2.4. The advent of full-waveform lidar systems

Waveform analysis allows one to set up advanced processing methods which increase pulse detection reliability, accuracy and resolution. Furthermore, the new technology of full-waveform lidar systems gives more control to the end user in the interpretation process of the physical measurement. It provides additional information about the structure and the physical backscattering properties of the illuminated surface (reflectance and geometry).

The first truly operational topographic system, LVIS (see Section 3.2 for more details) appeared in 1999 and demonstrated the value of recording the entire waveform for vegetation analysis (Blair et al., 1999). The first commercial full-waveform lidar system appeared in 2004 (Hug et al., 2004). Section 3 gives a comprehensive list of the names, manufacturers and characteristics of such laser scanning systems.

Full-waveform systems sample the backscattered waveform at a frequency of around 1 GHz. They allow one to determine the vertical distribution of targets hit by a laser pulse.

The understanding of such waveforms requires a pre-processing step. On the one hand, waveforms can be decomposed into a sum of echoes to generate a 3D point cloud (Section 4). Resulting data can then be used in classical lidar algorithms (classification, building reconstruction, etc.). On the other hand, new approaches are also conceivable. They are based on the captured waveforms using a "1D signal topology" instead of a 3D point cloud (*cf.* part 6.2).

2.2.5. Recording full-waveform data

To record the waveform, *i.e.* the laser backscattered energy as a function of time, lidar manufacturers have added digitization terminals to their systems and hard disks with high storage capacity. The waveforms are usually digitized on 8 bits. The volume of data is bound to be five times superior to the 3D point cloud over the same area. The main limitation of surveying areas with a full-waveform lidar system is subsequently the storage capacity. For example, the Optech ALTM 3100 device is able to collect data during 3 h and 20 min with a 300 GB hard drive, with a PRF equal to 50 kHz.

The two main techniques for recording the signals are described in Jutzi and Stilla (2003).

Whatever the lidar system method, the constant digitization sampling period varies between 1 and 10 ns. The waveform is not integrally recorded but only for a predefined maximum number of samples. Indeed, it is necessary to avoid massive storage problems. For example, Optech ALTM systems can store up to 440 samples for each pulse. This is equivalent to a discrete vertical section of 66 m (440×0.15 m per sample). The TopEye MarkII system saves 128 samples according to a predefined mode which is either "*first pulse and later*" (127 samples after the first) or "*last pulse and earlier*". It means that full-waveform systems will not record, within a given waveform, both echoes from the canopy and from the ground, if the trees are taller than the maximum "recording length" of the system.

The present issue with full-waveform data deals with data handling and management since much larger data volume are now recorded.

3. Typology of full-waveform lidar systems

The first full-waveform systems were designed in the 1980s for bathymetric purposes (Guenther and Mesick, 1988). Topographic devices appeared in the mid-1990s with experimental systems and have been commercially available for a few years. Full-waveform topographic lidar systems mainly differ in footprint size, pulse energy and PRF. Small-footprint and large-footprint systems do not collect the same information over the same area. The applications therefore differ from a system to another.

Most commercial systems are small-footprint (0.2–3 m diameter, depending on flying height and beam divergence) with higher PRF. They provide a high point density and an accurate altimetric description within the diffraction cone (Fig. 3(a)). Nevertheless, mapping large areas requires extensive surveys. Besides, small-footprint systems often miss tree tops. It is difficult to

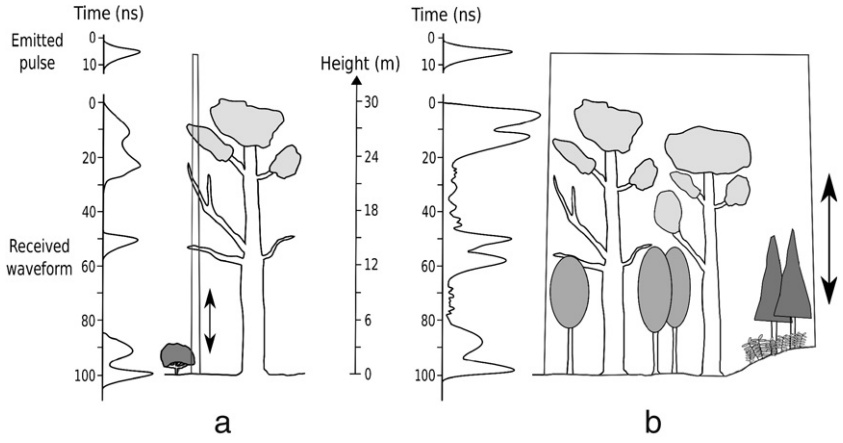

Fig. 3. Transmitted and received signals in a wooded area with (a) a small-footprint lidar and (b) a large-footprint lidar. With a small-sized footprint, all targets strongly contribute to the waveform shape but the laser beam has a high probability of missing the ground. When considering large footprints, the last pulse is bound to be the ground but each echo is the integration of several targets at different locations and with different properties.

determine whether the ground has been reached under dense vegetation. Consequently, ground and tree heights cannot be well estimated (Dubayah and Blair, 2000).

Large-footprint systems (10–70 m diameter) increase the probability to both hit the ground and the canopy top. They avoid the biases of small-footprint systems. Thus, the return waveform gives a record of the vertical distribution of intercepted surface within a wider area (Fig. 3(b)). The first experimental full-waveform topographic systems were large-footprint and mostly carried by satellite platforms. With a higher flying height, pulses must be fired at a lower frequency and with a higher energy.

3.1. Bathymetric lidar systems

Designed for accurate sea-depth determination, they are composed of two beams, one green (532 nm) and one infrared (1064 nm). The green beam traverses the air-water interface and propagates in the water until the sea bottom with the least attenuation. The infrared beam is reflected by the water and gives the range from the plane to the sea surface. Bathymetric waveforms are therefore composed of two peaks. Processing these waveforms consists of finding the two main signal maxima and deriving the range values. We will not go into further detail regarding bathymetric lidar systems in this article. More information is available in Guenther et al. (2000).

There are currently several bathymetric lidar systems: **LARSEN-500**, the very first bathymetric system, **LADS** (Laser Airborne Depth Sounder), the **SHOALS** series (Scanning Hydrographic Operational Airborne Lidar Survey), fully operational since 1994, **Hawk Eye**, developed in Sweden on a model similar to SHOALS and **EAARL** (Experimental Advanced Airborne Research Lidar), developed by NASA in 2002. Their main characteristics are described in Section 3.4.

3.2. Experimental lidar systems

The following prototypes developed by NASA have been designed to assess the characteristics of woodlands or land cover. They aim at mapping large areas to provide data at a resolution of several meters and a swath width up to 1–2 km.

- *Scanning Lidar Imager of Canopies by Echo Recovery (SLICER)*: the precursor of the topographic systems described below was designed to characterize the vertical structure of the canopy. This medium-sized footprint airborne device demonstrated that full-waveform systems could be used to assess the characteristics of woodlands, distinguish tree ages and species, and characterize the structure of extensive areas (Lefsky et al., 1999b). SLICER data can be downloaded on line (SLICER, 2008).
- *Shuttle Laser Altimeter (SLA)*: this satellite sensor was designed to cover seas, clouds, and land (glaciology, tectonics, hydrology, geomorphology, etc.). Two versions were produced, SLA-01 and 02 (1996–1997), for a feasibility study for the future MBLA and GLAS systems. SLA-02 was used to verify the accuracy of a global 1 km resolution DTM and thus characterize some systematic biases (Harding et al., 1999).
- *Laser Vegetation Imaging Sensor (LVIS)*: this improved version of SLICER was used to test and provide data for developing algorithms, calibrating instruments and evaluating the performance of measurements to assess the future Vegetation Canopy Lidar (VCL) mission (*cf.* MBLA system). It also demonstrated the potential of full-waveform data to characterize woodland areas and measure the Earth's topography, even below the canopy (Blair et al., 1999). It was mainly used to develop a real-time algorithm for classifying ground points by analyzing the return waveform. Sample data from this system are public (LVIS, 2008).
- *Multi-Beam Laser Altimeter (MBLA)*: the MBLA system was part of the VCL mission (Vegetation Canopy Lidar). VCL is an active space-based lidar remote sensing system consisting of a five beam instrument with 25 m contiguous along track resolution. VCL aimed at providing data sets for understanding major environmental issues (climatic change, sustainable land use), and improving global biomass and carbon stocks estimation. VCL's core measurement objectives were canopy top heights, vertical distribution of intercepted surfaces and ground surface topographic elevations (VCL, 2008). This programme was due to be launched in 2003 but was abandoned.
- *Geoscience Laser Altimeter System (GLAS)*: the five year ICESat satellite mission, carrying GLAS sensor, was launched in January 2003 to study the evolution of land and sea glacial masses in the Antarctic and Greenland, the roughness and thickness of sea ice, the topography (using a 1064 nm laser) and the vertical structure of clouds and aerosols (532 nm laser) (Geophysical Research Letters, 2005; GLAS, 2008). ICESat classifies the return waveform in real-time into land/ice and icesheet/sea by analyzing the return waveform and recognizing Gaussian distributions from which the main characteristics are extracted (Brenner et al., 2003). Data sets are available on the mission Web site (ICESat, 2008).

3.3. Commercial lidar systems

Operational versions of commercial full-waveform systems have been available since 2004. These small footprint systems have considerable potential but do not have any dedicated application (Hug et al., 2004). The manufacturing companies are Riegl (Austria), Toposys (Germany), TopEye/Blom (Sweden) and Optech (Canada). Leica (Switzerland-Germany) ALS-series do not currently have a full-waveform digitizer but are working on it.

3.4. Technical specifications of the main existing systems

Tables 1 and 2 summarize the main characteristics of the full-waveform lidar systems mentioned above.

Notes:

- *Final year*: blank if the system is still in use.
- *Wavelength*: when two wavelengths are given (typically 1064 and 532 nm), this means that the system includes two lidar systems, each with its own wavelength. These are either bathymetric applications or satellites with dual coverage (land and sea).
- From *Flying height* to *Range accuracy*: the characteristics are given as ranges of values. These are manufacturer's data and are limited by the system's flying height. The formulas for determining the exact values for a given height can be found in Baltsavias (1999b).
- *Range accuracy*: this is the accuracy given by the manufacturers after on-line peak detection in the return waveform (telemeter accuracy). It is distinct from the along-track minimum distance between two consecutive peaks and from the altimetric accuracy of lidar data.
- In a cell, "-" means that the information is unknown or not available.

4. Processing the backscattered waveform

4.1. Existing approaches

Two approaches are conceivable for processing the vertical profiles recorded by the new generation of airborne lidar sensors. On one hand, it consists of decomposing the waveform into a sum of components or echoes, so as to characterize the different targets along the path of the laser beam. The aim of this approach is to maximize the detection rate of relevant peaks, to generate a denser 3D point cloud and, finally, to extend waveform processing capabilities by fostering information extraction from the raw signal. Increasing the number of 3D points is of interest for forestry applications (*cf.* Section 6.1.1). Extracting more information can be useful for segmentation and classification purposes, in both forested and urban areas (see Section 5).

On the other hand, the whole 1D signal is preserved. A spatio-temporal analysis is applied to find features within a 3D waveform space. This approach is suitable for urban areas where the geometry is regular (*cf.* Section 6.2).

The latter approach has been barely investigated. Most research on full-waveform analysis has been focused on the enhanced 3D point cloud. This section therefore deals with waveform decomposition. If advanced techniques are efficient to extract strong and weak echoes and for range determination (Section 4.2), other approaches model the waveforms using analytical functions (Section 4.3).

4.2. Range determination and echo extraction

4.2.1. A deconvolution approach for range determination and target discrimination

Based on a physical understanding of the pulse propagation and its interaction with the illuminated surface, Jutzi and Stilla (2006) propose a relevant algorithm to discriminate different surface responses which are very closely located in range (<0.15 m).

First, the received waveform of the backscattered pulse is computed using the lidar equation (formula (5)). It depends on the transmitted waveform (modeled by a Gaussian function randomly modulated by a Gaussian noise), on the spatial energy distribution of the emitted pulse (also modeled, depending on the laser device), on the surface response (with given reflectance and geometric properties, here with two differently elevated specular plan plates), on the atmospheric transmission, and receiver efficiency. Then, the waveform is processed in four main steps:

- pulse detection with a noise dependent threshold;
- deconvolution in the Fourier domain of the transmitted waveform with the received waveform;
- estimation of the surface function using the Wiener Filter; the Wiener Filter is a real function estimated from the modulated transmitted waveform and the background noise;
- waveform fitting with the Levenberg–Marquardt technique using the surface function as modeling function (see part 4.3.2).

Finally, experiments on different kinds of surfaces show that surfaces with a distance corresponding to less than 0.15 m can be resolved.

4.2.2. Advanced echo extraction methods

The main reason for decomposing the waveform is to extract more points in a more reliable way. Several methods have been carried out so far. They are described in this section. Waveform fitting algorithms, described in Section 4.3.2, also permit to find peak location and echoes undetected by traditional pulse detection methods. However, they require to model the echoes with an analytical function. But an inappropriate model can lead to erroneous results.

- *Detection of weak pulses*. Stilla et al. (2007) show it is possible to detect weak pulses corresponding to partially occluded targets or objects with poor surface backscatter properties. A waveform stacking technique is performed by establishing neighborhood relationships between consecutive waveforms. Mutual information is therefore accumulated to produce a "global" scattering for such targets. This technique predicts new pulses not detected by standard algorithms.
- *Improved range determination*. For urban landscapes, Kirchhof et al. (2008) propose a method to improve the point density, the range accuracy as well as the segmentation between partially penetrable objects and impenetrable surfaces. The goal of this approach is to fill gaps that can appear in partly occluded surface regions. Assuming that the laser beam hits a planar surface with a given slope, the surface response is modeled (transmitted and received waveforms are known) using a matched filter. It produces range values and generates a 3D point cloud. Points are segmented according to a given feature and those expected to belong to impenetrable surfaces are used to estimate surface primitives. A new surface response is finally computed and used as prior knowledge at the beginning of the algorithm.

  This method (as well as the deconvolution approach) allows one to determine the range of each echo without any pulse shape assumption and to detect weak echoes corresponding to partially occluded and partly illuminated regions.

Table 1
Main technical specifications for full-waveform lidar systems.

System	Company manufacturer	Platform	Beam deflection	Beginning–final year	Wavelength (nm)	Flying height (km)	Pulse rate (kHz)
Bathymetric							
LARSEN 500	Terra Surveys Optech	Airborne	Rotating mirror	1983–	1064/532	0.5	0.02
MarkII	LADS TopEye	Airborne	Fibers	1989–	1064/532	0.37–0.5	0.9
Hawk Eye	Saab Optech	Airborne	Oscillating mirror	1990–	1064/532	0.05–0.8	0.2
SHOALS 1000T	US army Optech	Airborne	Oscillating mirror	1994–	1064/532	0.2–0.4	0.4
EAARL	NASA	Airborne	Oscillating mirror	2002–	1064/532	0.3	3
Experimental							
SLICER	NASA	Airborne	Oscillating mirror	1994–1997	1064	<8	0.075
SLA-02	NASA	Satellite	None	1996–1997	1064	285	0.01
LVIS	NASA	Airborne	Oscillating mirror	1997–	1064	<10	0.1–0.5
GLAS	NASA	Satellite	None	2003–	1064/532	600	0.04
MBLA	NASA/University of Maryland	Satellite	Oscillating mirror	None	1064	400	0.01/0.242
Commercial							
LMS Q560	Riegl	Airborne	Polygon	2004–	1550	<1.5	≤100
Falcon III	TopoSys	Airborne	Fibers	2005 –	1560	<2.5	50–125
MarkII	TopEye	Airborne	Palmer	2004–	1064	<1	≤50
ALTM 3100	Optech	Airborne	Oscillating mirror	2004–	1064	≤3.5	≤70
ALS60	Leica	Airborne	Oscillating mirror	2006–	1064	0.2–6	≤50

Table 2
Main technical specifications for full-waveform lidar systems (*second part*).

System	Pulse energy (mJ)	Pulse width (ns)	Scan rate (Hz)	Scan angle (°)	Beam divergence (mrad)	Footprint size (m)	Range accuracy (cm)	Digitizer (ns)
LARSEN 500	–	12	20	30	4	2@500 m	30	1
LADS MarkII	7	–	18	27	–	–	15	2
Hawk Eye	2/15	7	0.3–7	0/40	2–15	1–7.5@500 m	30	1
SHOALS 1000T	2/15	6	0.3–7	0/40	2–15	0.8–6@400 m	15	1
EAARL	0.07	1.3	25	22	0.03	0.15@300 m	3	1
SLICER	–	4	80	–	2	10@5 km	11	1.35
SLA-02	40	8	–	–	0.3	85@285 km	150	4
LVIS	5	10	500	14	8	40@5 km	30	2
GLAS	75/35	6	–	0	0.11–0.17	66@600 km	5–20	1
MBLA	10	5	–	–	0.06	24@400 km	100	4
LMS Q560	0.008	4	5–160	45	0.5	0.5@1 km	2	1
Falcon III	–	5	165–415	28	0.7	0.7@1 km	–	–
MarkII	–	4	<50	14/20	1	1@1 km	2–3	1
ALTM 3100	<0.2	8	<70	50	0.3/0.8	0.3/0.8@1 km	1	1
ALS60	<0.2	5	<90	75 usually	0.22	0.22@1 km	2	1

4.3. Modeling and fitting the waveforms

When modeling the echoes within a waveform, a parametric approach is always chosen. Parameters of a mathematical model are estimated for each detected peak in the signal. These parameters provide additional information about the target characteristics (shape and reflectance) and extend waveform processing capabilities. Statistical elements extracted by signal processing techniques are the number of significant peaks, their range to the sensor and the parameters of the modeling function. A single function is always used to model all echoes of the waveforms.

One wishes to decompose a waveform $y = f(x_i)$ into a sum of n components:

$$y_i = \sum_{k=1}^{n} \phi_k(x_i) + b_i \tag{6}$$

where f is the waveform model, ϕ the echo model with a set of parameters $\boldsymbol{\theta}$ ($f = \sum_k \phi_k$), $\{x_i\}_{i=1,\ldots,N}$ is a sequence of uniformly-spaced points, $y = \{y_i\}_{i=1,\ldots,N}$ the sampled waveform, and b the noise.

A relevant echo model is particularly suitable so that related parameters should be used for segmenting the 3D point cloud. A large body of literature addresses the issue of fitting waveforms with a given parametric model.

4.3.1. Modeling the waveforms

A waveform is a convolution between a laser transmitted pulse (assumed to be of Gaussian shape with a calibrated width) and a "surface" scattering function, often considered as a Gaussian function (Wagner et al., 2006). The received signal is then assumed to be a mixture of Gaussian distributions. Such modeling is the most frequently used to process full-waveform data. The analytical expression of the Gaussian function is:

$$\phi_k(x) = A_k \exp\left(-\frac{(x-\mu_k)^2}{2\sigma_k^2}\right) \tag{7}$$

where A_k is the pulse amplitude, σ_k the pulse width, μ_k the pulse range. Thus, $\boldsymbol{\theta}_k = \{A_k, \sigma_k, \mu_k\}$.

The Gaussian model is sufficient for most applications, especially for large-footprint lidar data (Zwally et al., 2002; Wagner et al., 2006). However, for small-sized and medium-sized footprints, this model is not always justified. In urban areas, many

peaks are distorted: indeed, most of the return waveforms are subject to the mixed effects of geometric (*e.g.*, roof slopes) and radiometric object properties (*e.g.*, different kinds of street and roof materials). Hence, the characteristics of return peaks may differ significantly. Consequently, other modeling functions have been proposed in Chauve et al. (2007). For instance, it has been shown that the generalized Gaussian function, which is an extension of the Gaussian function, improves signal fitting and models distorted peaks.

4.3.2. Fitting the waveforms

Several methods have been carried out to fit the waveform with a single modeling function:

- Non-linear least-squares approach using Levenberg–Marquardt optimization algorithm,
- Maximum likelihood estimate with *Expectation–Maximization* algorithm,
- Stochastic approach using Reversible Jump Monte Carlo Markov Chain method.

► *Non-linear least-squares approach*. Hofton et al. (2000) give a description of a non-linear least-squares method which is used in bathymetric (Wong and Antoniou, 1991), satellite (Brenner et al., 2003), terrestrial (Jutzi and Stilla, 2006) and airborne laser scanning systems (Duong et al., 2008; Reitberger et al., 2008a).

This problem is a system of N observations with $m \times n$ unknown parameters. $m = \text{card}\,\boldsymbol{\theta}$ is the number of parameters of the modeling function and n the number of echoes. The quality of the results is evaluated by a variable ξ. One aim at fitting the data with a prescribed accuracy ϵ.

$$\xi = \sqrt{C \sum_{i=1}^{N} (f(x_i) - y_i)^2} < \epsilon \tag{8}$$

where C is a weight: $C = 1/N$ in Hofton et al. (2000) or $C = 1/(N - \text{card}\,\boldsymbol{\theta})$ in Chauve et al. (2007).

The system is solved using a non-linear least-squares method, the Levenberg–Marquardt (LM) technique (Marquardt, 1969). An iterative algorithm is used. There is no algorithm for solving the problem directly since the $\{\phi_k\}_k$ are not linear functions. The LM algorithm is known to be robust but requires a good initialization step.

Initial values are mainly provided by traditional pulse detection methods (Wagner et al., 2006). Besides, raw waveforms are noisy and are sometimes smoothed. The intensities above a threshold are considered to be potential echoes. Moreover, to overcome the problem of a wrong initialization step, Hofton et al. (2000) add progressively peaks in the least-squares fitting algorithm according to their amplitude until ξ is greater than a given threshold. Chauve et al. (2007) propose an iterative approach: after coarse peak detection, missing peaks are found in the difference between the modeled and the initial signals. If new peaks are detected, the fit is performed again. This process is repeated until no further improvement is possible.

► *Maximum likelihood approach: the EM algorithm*. Persson et al. (2005) have developed a pulse detection method based on the Expectation–Maximization algorithm (EM) (Dempster et al., 1977). The EM algorithm is a two-stage iterative optimization technique for finding maximum likelihood solutions. EM alternates between performing an expectation (E) step, which computes an expectation of the likelihood, and a maximization (M) step, which computes the maximum likelihood estimates of the parameters by maximizing the expected likelihood found on the E step. It consists in computing, for each sample, the probability of belonging to one of the kth distributions which decomposes the signal. Parameters found during the M step are then used to begin another E step, and the process is repeated. This method is a general technique. They assume that the return waveform is a sum of Gaussians. Nevertheless, it is possible to choose other probability density functions to fit the return waveforms.

► *Reversible Jump Monte Carlo Markov Chain method*. Levenberg–Marquardt and Expectation–Maximization algorithms require the explicit gradient expression of the modeling function. This is a drawback for complex analytical functions: the first derivative for all parameters is not always computable. Moreover, it has already been shown that the more parameters to be estimated, the more inconsistent fitting results appear (Chauve et al., 2007). Hernández-Marín et al. (2007) have proposed a method to fit terrestrial lidar waveforms with a specific modeling function (a set of four piecewise exponential functions), that can be adapted to geospatial topographic waveforms. For that purpose, the Reversible Jump Monte Carlo Markov Chain (RJMCMC) method is used. A grammar of functions can be defined and this optimization algorithm will find the best model. It can even find the best mixture of functions with the optimal parameters (Green, 1995). The fitting algorithm is based on the formulation of an energy, allowing the introduction of prior knowledge related to the object layout (*e.g.*, surface reflectance) and to the waveform decomposition (the number of echoes can be limited). Consequently, a signal fitting algorithm using the RJMCMC technique is relevant: it is robust (the global minimum of the energy is found), no initialization and no gradient are required, and the grammar of models is extensible.

4.4. Conclusions

The literature shows that the main process applied to lidar profiles is signal decomposition and modeling. The advantages of waveform processing is threefold. First, the different algorithms presented in the previous sections no longer limit the number of peaks that can be detected. Additional points are therefore extracted. As expected, it concerns those with low intensity, located where multiple echoes appear, or overlapping echoes (*cf.* Fig. 4 and all papers cited in this section). Such points are not recorded by a conventional multiple pulse system due to internal thresholds for peak detection. Consequently, on forested areas, waveform processing can for instance provide up to 60% more pulses than real-time system (Reitberger et al., 2008a; Chauve et al., in press). This result depends on the tree species, the leaf-on/leaf-off conditions and the survey specifications. Figs. 5 and 6 show on a profile and on different tree species additional points that can be extracted. In urban areas, new peaks are found in the tree canopy as well as on building edges. When the laser beam hits an edge, a low amplitude pulse corresponding to the ground can appear after the roof echo.

Second, waveform processing improves object range determination, even over complex surfaces (Zwally et al., 2002). For instance, in forested areas, both canopy and ground height estimates can be improved (Duong et al., 2008) but this result depends on the survey specifications and the landscape (Chauve et al., in press). In urban areas, range accuracy of solid opaque targets can also be bettered (Kirchhof et al., 2008). Consequently, the modeling of the landscape is improved: the processing of Digital Terrain and Digital Surfaces Model from point clouds take advantage of the better height determination.

Third, modeling the echoes provide additional parameters that can be useful for classification purposes (see Section 5).

The Gaussian approximation is shown to be satisfactory and sufficient for most of mapping applications in urban and

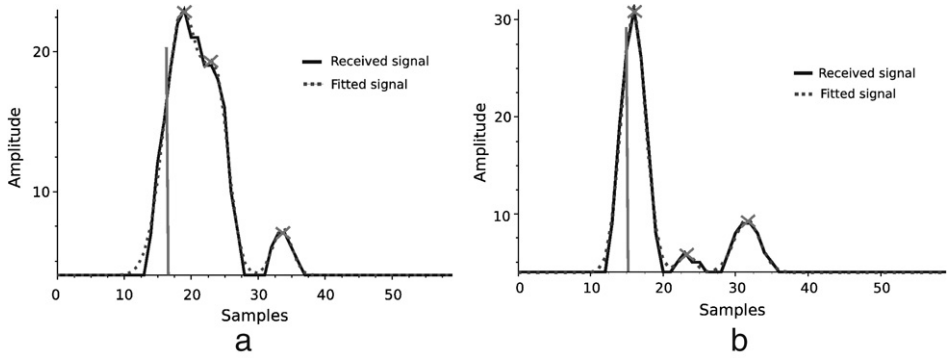

Fig. 4. Improvement of lidar waveform peak detection. (a) Waveform with two overlapping pulses: three pulses are detected with two overlapping ones. (b) Waveform with low intensity pulse: three pulses are detected with two of low amplitudes. In both signals, only one echo is found by hardware processing (vertical line). The crosses indicate the pulse location with post-processing.

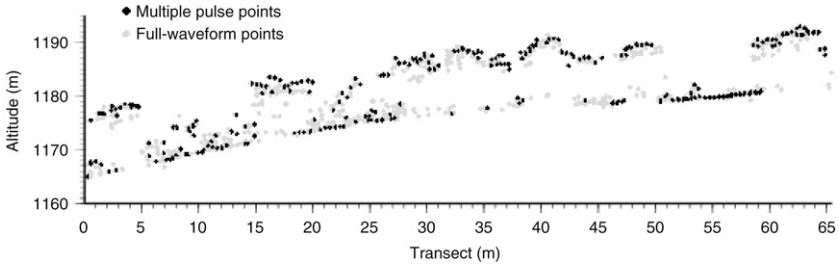

Fig. 5. Comparison over a vegetated area between full-waveform lidar points and multiple pulse lidar points.

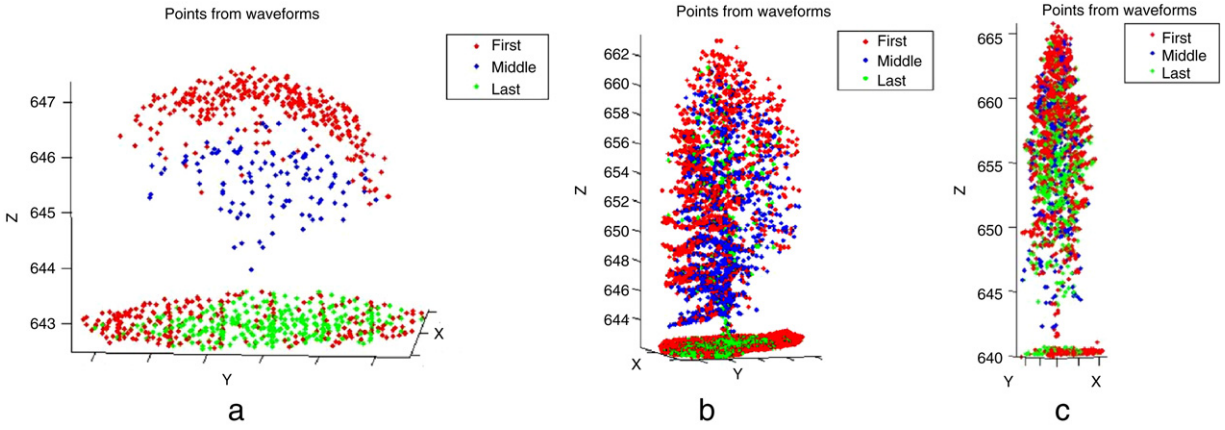

Fig. 6. Extracted points on different tree species from full-waveform data post-processing. (a) Deciduous (leaf-on). (b) Deciduous (leaf-off). (c) Coniferous. Red, green and blue points correspond respectively to the first, last and intermediate extracted pulses (Reitberger et al., 2008a).

vegetated areas, both for large-footprint and small-footprint lidar data (Hofton et al., 2000; Wagner et al., 2006). Wagner et al. (2006) show that fitting Gaussians to the echoes is however less satisfactory for high amplitudes. Furthermore, for low amplitude pulses, the estimation of the echo parameters is less accurate. Other models, such as the generalized Gaussian function, may be of interest.

5. Quantitative analysis of return waveforms

The signal processing step fits echoes with appropriate modeling functions: their parameters contain significant information on the roughness, slope and reflectivity of the hit surfaces. For segmentation and classification purposes, many studies have already been carried out to evaluate the effect of the transmission and reflection parameters of the signal on the shape of the waveforms. They are described below. Studies of the laser system calibration and intensity correction are also presented.

5.1. Behavior of a reflected waveform

Many elements which could modify the shape of the waveform have been studied so far by many authors:

Distance to the sensor and emission angle: Vandapel et al. (2004) test different distance and angle configurations with a terrestrial sensor. At short distances from the target, the peak is asymmetrical, with a long rise and a short trail. It becomes symmetrical as the distance increases. Variations in the shape are also noticed with changes in the angle of incidence. The smaller the angle, the narrower and more symmetrical the peak.

Roughness: different responses are noticed between smooth surfaces (one or two echoes if there are discontinuities) and porous surfaces (multiple echoes at different depths, equivalent to the behavior of trees and vegetation) (Vandapel et al., 2004).

Geometry: The FOI (Swedish Ministry of Defence Research Institute) proposes a comprehensive laser data simulation model. It includes the detector characteristics, the target geometry and reflectivity, the atmospheric attenuation, etc. Steinvall (2000) and Carlsson et al. (2001) have carried out experiments on targets with simple shapes to study the combined effect of the geometry and target reflectance (mixture of diffuse and specular) on the return waveform. A significant spread in the pulse and a decrease in its amplitude are observed over flat surfaces when the incident angle increases (Fig. 7(a)). It can lead to an erroneous estimation of the distance, especially with abnormal angle of incidence. Besides, similar waveforms are observed between plane surface and corners. Consequently, two plane surfaces can be assimilated to a single one. Eventually, simulations were carried out on steps to investigate whether it was possible to resolve two close planar surfaces (Fig. 7(b)), and on different canopy shapes.

A comparison of the return waveforms reflected by various shapes shows the potential advantage of classifying objects by analyzing the full waveform from a single pulse. However, it must be pointed out that these conclusions are based on the major assumption that the target exhibits Lambertian reflectance.

Geometry + radiometry: Jutzi and Stilla (2003) set up experiments to assess the effect of various urban materials on the return waveform. Images of range, amplitude and pulse width are calculated for pebbles, corrugated iron, slanted slate plate and flat roof tiles (Fig. 8). The four types of roof material tested behave in different ways. This confirms that it is not possible to classify waveforms simply as vegetation/buildings/roads. Similar responses are recorded between objects of different classes. Besides, there is significant deviation within the same class. This study is similar to that described for example in Lachérade et al. (2005) on the study of the variation in reflectance of various urban materials (asphalt, tar, concrete, granite, etc) using high resolution aerial photographs.

Other factors: Carlsson et al. (2001) have noticed that atmospheric and specular effects on the target are negligible on the range measurement compared with the other effects.

5.2. Echo classification

Displaying a 3D point cloud generated from full-waveform data with model parameters does not allow one to interpret the results simply (see Fig. 9) (Hug et al., 2004; Ducic et al., 2006). Nevertheless, it is possible to define some particular behavior for several objects. The echo is wider on the canopy or ploughed fields compare with roads or meadow areas. High amplitudes are noticed on grass and bare earth and variable amplitudes on the roofs of buildings, depending on the roof materials (Fig. 10). Moreover, weak echoes are wider and the intensity of additional extracted points is, predictably, lower than for the first echoes.

However, a point cloud obtained by one of the methods described in Section 4 cannot be classified categorically, even with additional features and hints about the knowledge of the influence of each object. A wide echo with low amplitude does not necessarily come from vegetation. Fig. 10 shows that over vegetated areas the pulse widths are included in a large range of values. Roads and building roofs are made from different types of material and, therefore, have different characteristics. The features currently extracted from a modeling step often have values similar to natural objects (Gross et al., 2007; Mallet et al., 2008). Consequently, simple classification algorithms, *e.g.* classification tree with empirical thresholds, lead to a high rate of incorrect classification (Duong et al., 2006; Ducic et al., 2006). A reliable approach to detect vegetated areas is proposed in Gross et al. (2007), based on the eigenvalues of the covariance matrix computed for each point with the intensity values in a cylindric environment. However, geometric features are used in addition to waveform features for the discrimination. Other features have to be found to classify full-waveform point clouds. Attributes, such as the cross-section or the backscattering coefficient, which describe the scattering properties of the targets, seem valuable to retrieve these physical characteristics and improve segmentation/classification results (Wagner et al., 2008b).

Moreover, in order to exploit pulse shape parameters, we have to bear in mind that the shape of the nth pulse of a waveform depends on the scattering characteristics of the $n-1$ first echoes. It is known that the cross-section of the nth target is expected to decrease depending on its "rank" in the waveform, but it is not straightforward to predict how (Wagner et al., 2008a).

Eventually, it is still difficult to quantify specifically both geometric and radiometric influences of a target on the return waveform. Since in reality this information is correlated, it is all the more a challenging task.

Large-footprint lidar data can nevertheless provide coarse classification results since small surface variations are discarded. Indeed, ICESAT system provides real-time classification from statistical analysis of the backscattered waveforms (Brenner et al., 2003). The return signals are fitted by a sum of Gaussian distributions. The extracted parameters are compared with theoretical waveforms for different surfaces, likely to be statically representative of these surfaces. Return waveforms can therefore be classified as land, ice sheet, sea ice or ocean. The backscattered signal is a mean of individual responses of encountered surfaces since the GLAS sensor footprint is 70 m wide.

5.3. Calibration and correction of laser intensity data

Intensity is not yet a clearly defined term (Wagner et al., 2008b). The echo amplitude is most commonly referred to as *intensity*. However, the intensity should be associated with the total energy of the echo (*i.e.*, $I = \sqrt{2\pi}\,A\,\sigma$ for a pulse of Gaussian shape, where A is the amplitude and σ is the width). The echo amplitude depends on many factors: target characteristics, lidar system, scan geometry, etc. Fluctuations can be noticed on large data sets between surveys, for instance due to different atmospheric conditions, and even between flight strips. The intensity/amplitude values provided by commercial lidar systems as well as those extracted from waveforms processing are neither calibrated nor corrected. Few studies have been carried out so far on intensity calibration and correction. They aim at converting intensity to a relative but comparable measurement for different epochs with different conditions, *e.g.*, for multi-temporal analysis or classification.

5.3.1. Calibration

The Finnish Geodetic Institute (FGI) has first proposed methods using calibrated targets with given reflectance to study the effect of the albedo on the shape of the return waveform and their directional properties (Kaasalainen et al., 2005a). Results show that reflectance plays a predominant role on the amplitude and width of the peak. The influence of the albedo cannot be separated from other target properties. However, the calibration protocol makes it possible to use intensity as data in its own right. Besides, a laboratory study was carried out on various targets (Kaasalainen et al., 2005b). The materials tested are sand with various grain

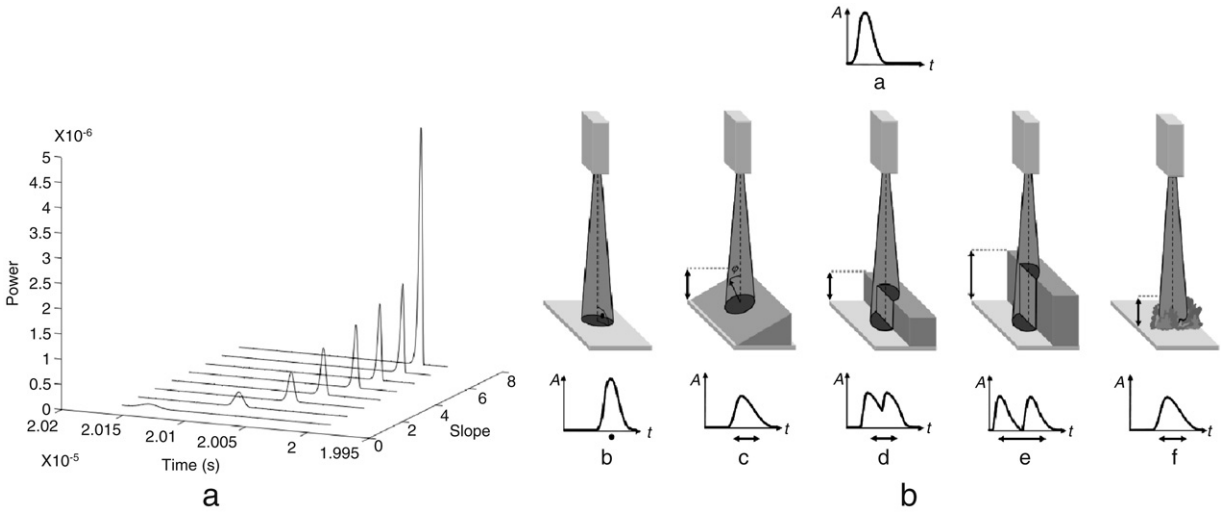

Fig. 7. Examples of the effect of specific targets on the return waveforms. (a) Return waveforms for eight different target with decreasing slopes (Carlsson et al., 2001). (b) Waveform behavior for different targets with a given emitted pulse (Jutzi and Stilla, 2006).

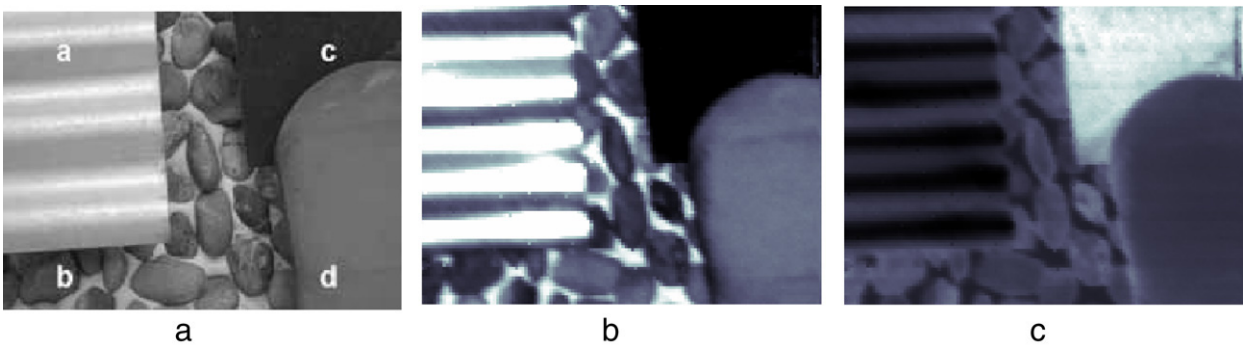

Fig. 8. Urban material influence on the shape of the return waveforms (Jutzi and Stilla, 2003). (a) Urban materials tested. *a*: corrugated iron — *b*: pebbles — *c*: slanted slate plate — *d*: flat roof tiles. (b) Intensity image (black/low intensity → white/high intensity). (c) Pulse width image (black → white).

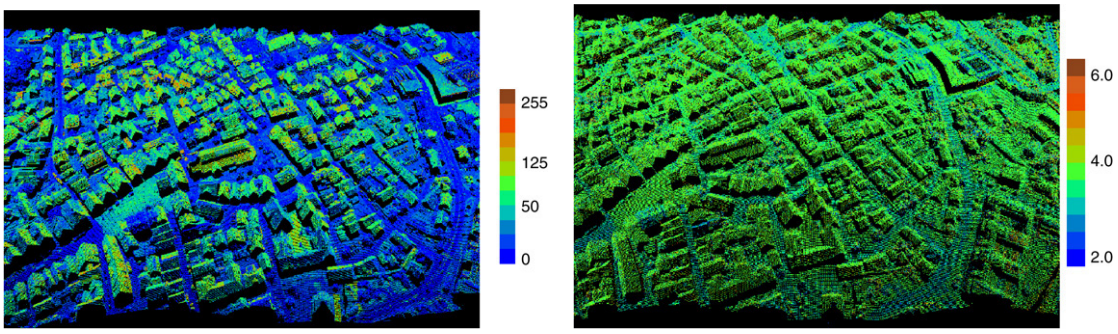

(a) Amplitude. (b) Width (ns).

Fig. 9. 3D point cloud display on an urban area with vegetation.

sizes, asphalt, trees, lichen and moss with small angle variations. Calibration is possible, but it proves difficult to define a reliable method to classify into various components based only on the intensity characteristics. The authors recommend studying much larger samples in the hope of drawing up an initial classification methodology.

Calibration can also be performed using the lidar equation (see Section 2.1.3 and Wagner et al. (2006, 2008b)) and external reference targets of known cross-section. For that purpose, the echo amplitude and width are needed. Therefore, only full-waveform sensors allow an accurate calibration for all target classes. No hypothesis is required.

5.3.2. Correction

Ahokas et al. (2006) show a strong correlation between the reflectance of surfaces and intensity for any flight height. Thus, the intensity value has to be corrected according to the scanning distance, the angle of incidence, the atmospheric transmission, the attenuation and power transmitted by the system. Certain flying heights are preferred (from 200 to 1000 m) for a suitable ground spot, as were scan angles less than 10°.

Furthermore, two methods for intensity correction are proposed in Höfle and Pfeifer (2007). The authors also review the papers considering lidar intensity for their research. A data-driven correction allows to globally correct data sets with different flying

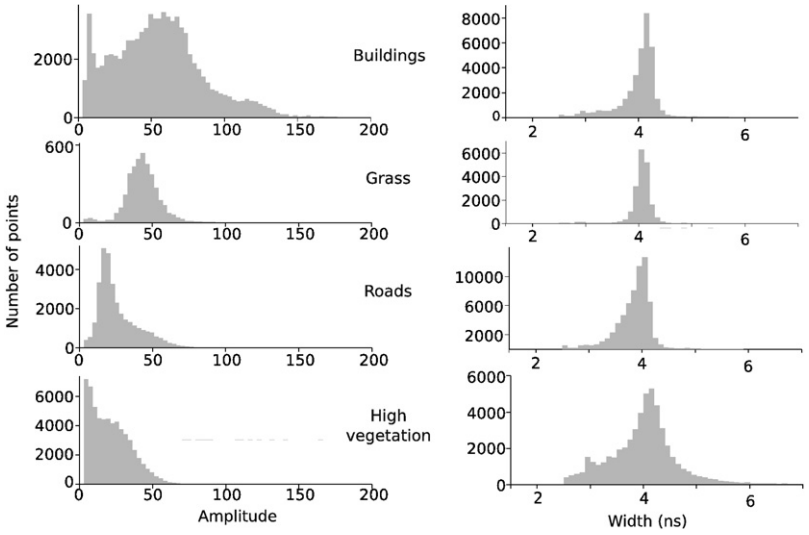

Fig. 10. Histogram of pulse amplitude and width for various urban classes.

heights thank to an empirical mathematical model. The function parameters are estimated using extended targets. Another correction is possible point by point, based on the lidar equation, knowing the same information as in Ahokas et al. (2006).

A number of hypothesis are made in these papers. Using full-waveform lidar data can overcome several issues of intensity correction. First, the angle of incidence is accurately known and the surface slope can be better estimated than with a conventional 3D point cloud (Kirchhof et al., 2008). Since the emitted pulse is recorded, it permits one to take emitted pulse intensity fluctuations into account. It is no longer needed to assume it constant (*cf.* Fig. 11). Finally, the target cross-section can be determined and the assumption of Lambertian reflectors removed (Höfle and Pfeifer, 2007).

6. Applications of full-waveform lidar data

6.1. Applications in woodlands

Full-waveform lidar data have been widely used for forest analysis. The waveforms are decomposed to produce dense 3D point clouds in the canopy which are then used to estimate forest parameters at the scale of the stand. Most of the literature on full-waveform systems deals with this topic. On one hand, one tries to benefit from a denser point cloud to improve forest parameter estimation. On the other hand, modeling is performed to understand the influence of forest parameters on the waveform shape.

Other works consider full-waveform data at the scale of the tree. For instance, tree stems can be detected (Reitberger et al., 2007), but a high point density is required to have enough points reaching the stems (see Fig. 6). Besides, tree crowns can be segmented in 3D, especially in the upper layer of the canopy (Reitberger et al., 2008b). Eventually, features provided by the waveform decomposition can be used in combination with geometrical attributes to classify deciduous and coniferous trees (Reitberger et al., 2008a). The results depend on the point density and the leaf-off/leaf-on conditions.

6.1.1. Estimating forest parameters

Many studies have already been carried out to estimate forest parameters using multi-echo lidar data: high point density can be used to extract trees in small areas, their height and crown diameter (Persson et al., 2002), their volume, to classify them according to species (Holmgren and Persson, 2004), to estimate their particular characteristics (Andersen et al., 2005) and even to measure the growth of the forest and detect trees that have been felled (Yu et al., 2004). Woodland parameters can be estimated at large scale: density of population, coverage, biomass, etc (Means et al., 1999).

Dubayah and Blair (2000), Lefsky et al. (2002) and Reutebuch et al. (2005) present the main studies with multi-echo and full-waveform airborne lidar for forestry applications.

Full-waveform lidar metrics are used to estimate the following woodland parameters:

- *Canopy height*: modeled from the measurement of the difference between the height of the first and last echoes, for different types of forest (temperate, boreal and tropical), at the tree or the stand levels (Lefsky et al., 1999a; Kimes et al., 2006). It is generally underestimated by at least one meter.
- *Vertical distribution of canopy material*: essential to determine other canopy features such as the above-ground biomass, predicting the state of the forest and determining the age of a plantation (Lefsky et al., 1999a).
- *Canopy height profile*: directly derived from the vertical canopy distribution for any deciduous forest. It defines the occlusion rate of a plantation (Harding et al., 2001).
- *Canopy cover*: obtained directly. This is the fraction of the signal reflected by the target corrected by the estimated ground reflectance (Means et al., 1999).
- *Canopy volume profile*: obtained by modeling. It can show the qualitative and quantitative differences between different ages of a given species (Lefsky et al., 1999a). It can also provide information on vertical leaf profiles (Harding et al., 2001).
- *Above-ground biomass*: modeled from the tree height measurements. This correlation was shown in mixed coniferous/deciduous areas, in mountains and in dense boreal and tropical forests (Drake et al., 2002; Hyde et al., 2005).
- *Basal area*: cross sectional area of the trunk, at DBH (Diameter Breast Height *i.e.*, 1.37 m) (Lefsky et al., 1999b; Means et al., 1999).
- *Mean stem diameter*: tree height is strongly correlated to the stem diameter (Drake et al., 2002). Allometric equations allow one to derive the stem diameter according to the canopy height and the tree species.
- *Crown and stem volume*: these features are inferred. The crown volume (tree parameter) is computed knowing the canopy volume (stand parameter), the tree density and species. The stem volume is inferred according to the mean stem diameter and the three height.

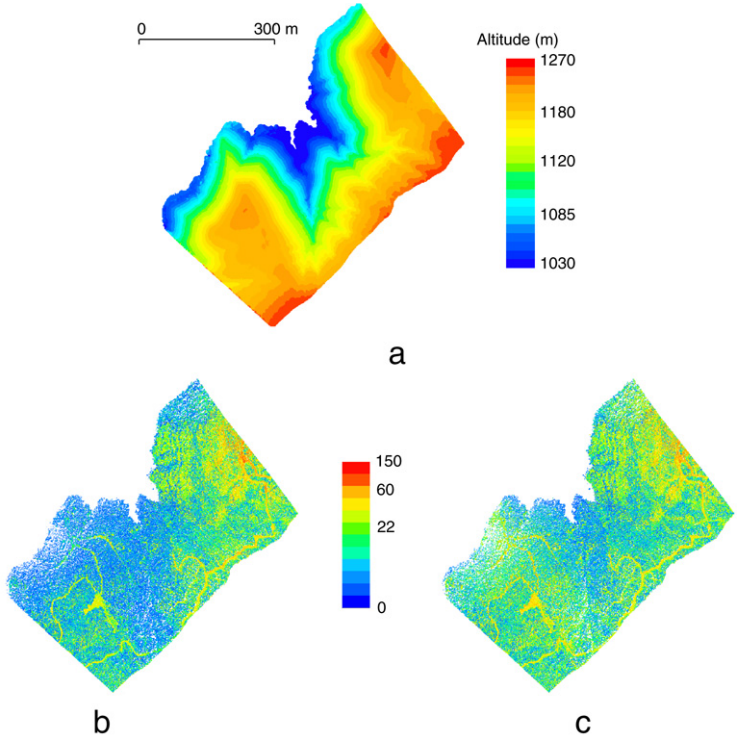

Fig. 11. Correction of the amplitude value using full-waveform data in a mountainous area: both effects of the angle of incidence and the transmitted pulse amplitude variations are taken into account. (a) DTM of the area. (b) Before correction. (c) After correction.

– *Other parameters*: the density of large trees can be inferred. Other additional data (thermic, optical, radar) is required for a satisfactory determination of the Leaf Area Index (LAI) and to have a knowledge of the tree species. It appears possible to classify species (Reitberger et al., 2008a) but a reliable algorithm has yet to be implemented.

Certain variables are obtained using allometric equations and vary according to the type of forest and their main characteristics (Hyde et al., 2005). Some parameters cannot be obtained or with low accuracy. It is therefore difficult to obtain a comprehensive estimation of forest parameters (even for main parameters such as tree height and crown diameter), and consequently parameters inferred as well as general relationships between structural forest variables for a given type of biome (and *a fortiori* for all types). Metrics derived from full-waveform data are not always significantly correlated with forest structural characteristics at the tree level, even if it works well for some forest types (Anderson et al., 2006).

First works dealing with forest change parameters have been carried out with large-footprint lidar data (Duong et al., 2008). Differences, in maximum canopy height for instance (0.5 m), have been noticed between summer and winter data.

Finally, forest parameter retrieval on steeped areas has to be mentioned. The height of the upper layer of the tree canopy, located in thalwegs for instance, can be the same as the higher ground parts of the terrain. In case of erroneous DTM, several forest parameters, such as the canopy height, crucial for modeling and inferring other features, will be incorrect. It would be consequently of interest to introduce waveform features, such as pulse amplitude and width, to improve ground/off-ground segmentation algorithms and derive more reliable DTMs.

6.1.2. Modeling forested areas

Modeling forested areas is particularly difficult due to the strong geometric complexity of the internal structure of the trees. Several studies have been carried out on this topic, mainly with large-footprint lidar data. Waveforms are generated over large areas (footprint superior to 10 m) in order not to take small tree elements into account. A tree model with a high level of details (leaves) is therefore not necessary.

Blair and Hofton (1999) give one of the first methodological developments for modeling forest scenes by simulating full-waveform lidar data. They simulate waveforms by breaking down the surface hit into small surfaces with their own backscattering characteristics but with the same reflectivity (typical of dense forest). A strong correlation between this data and that from the LVIS sensor is obtained. They show that the unmodeled effects such as multiple retrodiffusions do not make a significant contribution to the shape of the return waveform.

Sun and Ranson (2000) propose a more comprehensive model linking full-waveform data to the spatial structure and to optical properties of the vegetation. They simulate a forest where each tree can be parameterized by its height, its species and its maximum diameter. The return waveforms are simulated by dividing the 3D scene into small cells, with specific characteristics. Full-waveform data are then simulated with different tree species and ages and then compared to terrain data and SLICER samples. The simulations show that the model can be used to find main lidar signatures. It also shows that a lidar signal provides an indication of forest populations for both horizontal and vertical structures. It has also been noticed that the age and species of tree have a considerable effect on the waveform shape.

A different study of the relationship between the waveform and the canopy structure parameters is proposed in Ni-Meister et al. (2001). The arrangement of the structure on this relationship is taken into account to determine the 3D vegetation parameters. This is an adaptation of a hybrid geometric optical radiative transfer model (called GORT), to describe the effects of these parameters on the radiation environment (Ni-Meister et al., 1997). GORT describes the waveform as a function of the canopy parameters, which was checked against SLICER data. The lidar

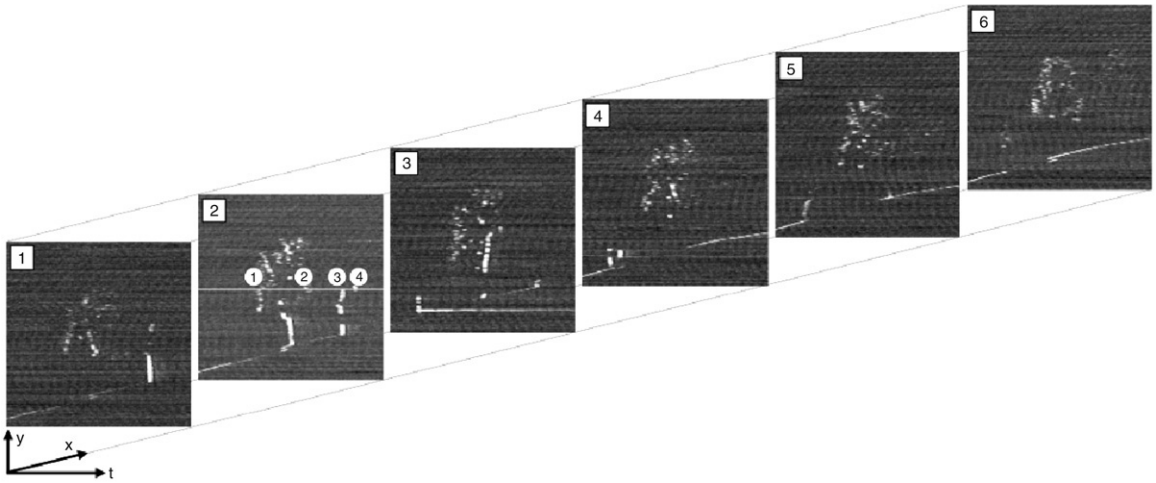

Fig. 12. Vertical sections in the $(y-t)$ plane of a lidar data cube with vegetation, ground and buildings. Numbers 1 to 4 indicate the echoes found in the second slice on the left (vegetation: *center* and building: *right*) (Stilla and Jutzi, 2008).

equation is used to determine the probability that a gap above a given height in the canopy appears. Besides, the authors propose a Directional Gap Probability Function to represent the probability that a laser beam reaches a certain point of height without being reflected. Finally, the results of the model are confirmed by comparing SLICER and LVIS data (Peterson et al., 2001).

Koetz et al. (2006) use the 3D model proposed in (Sun and Ranson, 2000). The radiative transfer model is inverted to determine the forest biophysical parameters. Some parameters are set using in situ spectrometric measurements or approximations. Simulated data are used to establish the feasibility of the inversion and show that the parameters can, potentially, be deduced: the tree height is accurately estimated, unlike the other parameters such as the LAI and the vegetation coverage.

These methods do not take into account multiple scattering that can also affect the return waveform. The method described in Kotchenova (2005) considers possible model errors, in particular for a dense canopy. To solve this, a 3D radiative transfer model is applied to simulate the propagation of photons across the vegetation. The predictions obtained on various mixed forest sites are compared with SLICER data. The simulated signal does not always match the real backscattered signal, regardless of the tree species. The main limitation of the model comes from the formulation of the probability functions that quantify canopy structure.

6.2. Applications in urban areas

The contribution of full-waveform data is less obvious in urban areas than in woodlands since multiple pulses only appear when the laser beam hits building edges. Jutzi and Stilla (2003) show that it is possible to visually distinguish between different urban materials hit by a laser beam and concludes that in-depth processing is required to recognize objects (*cf.* Section 5.1). They use the concept of neighborhood between waveforms and extracted points to interpret their data. Henceforth, the interpretation of a 3D point cloud can be improved by spatial and temporal cross-correlation of the peaks in successive waveforms.

The well-known problem of detecting the building edges is covered in Jutzi et al. (2005). A scene is segmented in "boundary zones" and "internal zones" by a region growing technique using the number of pulses, amplitude and distance to the target. Precise results are obtained accurate to 1/10 to 1/12 of the point spacing. However, these results are obtained assuming uniform reflectance and flat "internal" areas.

Eventually, by analyzing the parameters of each echo and taking the relationships between adjacent waveforms into account, they distinguish vegetation and man-made structures and then extract characteristic lines for the objects found in the scene (Jutzi and Stilla, 2005b). A spatio-temporal measurement cube (x, y, t) (distance matrix detector) is first generated to show neighborhood relationships. The cube is then sliced in vertical sections in the $(y-t)$ plane to give 2.5D information and the required relationships (Fig. 12).

The aim is to detect 3D segments within this cube, assuming a scene with a flat surface perpendicular to the incident signal (*i.e.*, a facade). Aligning the neighborhoods along y gives $(y-t)$ planes of intensity distributions with, along the y axis, a parallel line of maximum value. Intensity images are obtained and are processed by line detectors (in this case, Hough transform).

7. Conclusion

Full-waveform lidar systems can provide a more in-depth description of ground topography. Commercial systems are now available. Many studies use this type of data and have demonstrated considerable potential.

Several parameters have a significant influence on full-waveform lidar performance. In forested areas, the laser footprint diameter is drawn by the survey strategy. A large coverage gives global parameters (canopy height) whereas a small footprint provides an accurate description of the altimetric distribution of the vegetation. Besides, the sampling rate varies from one system to another. One will not be able to discriminate two objects too closely overlapped if not enough samples are recorded. Finally, the algorithm for processing the waveforms has to be taken into account as a significant parameter since results are different from one method to another. The way the data are exploited interferes also in this decision.

Full-waveform systems can make two important contributions: signal decomposition and advanced pulse detection methods can accurately recover a larger number of echoes than embedded real-time systems. This leads to slightly denser point clouds and to a better range determination. Furthermore, by modeling the return waveform, other information can be extracted such as intensity and pulse width. These two values provide information on the geometry and the radiometry of the target.

Full-waveform data are mainly used for forestry since the first experimental full-waveform lidar systems were developed at first for this particular purpose. Their data have been used for more than ten years. They produce a more detailed description of vegetated structures. It is then possible to estimate, model, and infer forest parameters more reliably. Full-waveform data are also used for 3D

modeling of vegetated scenes in order to study the effect of various parameters on the return waveform and to check models that have been developed.

In urban areas, the potentialities of full-waveform lidar are less obvious, perhaps because little research has been carried out to exploit them. Full-waveform systems cannot penetrate rigid, opaque structures such as buildings. Future research will be more likely about analyzing additional features extracted from the waveform and establishing neighborhood relationships between successive echoes to classify urban scenes (fine detection of edges of roofs, exact separation between vegetation and buildings).

In conclusion, studies carried out on full-waveform lidar data use only part of the extracted information from the return signal. The intensity/amplitude is rarely used as it must be calibrated and corrected first. Moreover, to characterize scenes with the main items of extracted information from each peak, it is essential to know the effect of the geometry and radiometry of the objects on the signal. Many studies have already been carried out in urban and woodland areas but no general conclusion has been drawn. At the moment, it is not possible to know the material or species of tree without ambiguity using the full-waveform parameters. The geometric and radiometric effects need to be decorrelated to achieve this. There is no doubt this is the most promising line of research. New modeling functions and extensive waveform simulations are also likely to be required for that purpose.

Acknowledgements

The authors would like to thank Michel Kasser (ENSG, France), Uwe Soergel (IPI Hannover, Germany), Adrien Chauve (IGN-CEMAGREF, France), the reviewers for their helpful comments towards providing the clarity of this article as well as Boris Jutzi (FGAN-FOM, Germany) for fruitful discussion on waveform analysis.

References

Ahokas, E., Kaartinen, H., Hyyppä, J., 2003. A quality assessment of airborne laser scanner data. International Archives of Photogrammetry, Remote Sensing and Spatial Information Sciences 34 (Part 3/W13), 1–7.

Ahokas, E., Kaasalainen, S., Hyyppä, J., Suomalainen, J., 2006. Calibration of the Optech ALTM-3100 laser scanner intensity data using brightness targets. International Archives of Photogrammetry, Remote Sensing and Spatial Information Sciences 36 (Part 1) (on CD-ROM).

Andersen, H.-E., McGaughey, R., Reutebuch, S., 2005. Estimating forest canopy fuel parameters using LIDAR data. Remote Sensing of Environment 94 (6), 441–449.

Anderson, J., Martin, M., Dubayah, M.-L., Dubayah, R., Hofton, M., Hyde, P., Peterson, B., Blair, J., Knox, R., 2006. The use of waveform lidar to measure northern temperate mixed conifer and deciduous forest structure in New Hampshire. Remote Sensing of Environment 105 (3), 248–261.

Baltsavias, E.P., 1999a. Airborne laser scanning: Existing systems and firms and other ressources. ISPRS Journal of Photogrammetry & Remote Sensing 54 (2–3), 164–198.

Baltsavias, E.P., 1999b. Airborne laser scanning: Basic relations and formulas. ISPRS Journal of Photogrammetry & Remote Sensing 54 (2–3), 199–214.

Blair, J., Hofton, M., 1999. Modeling laser altimeter return waveform over complex vegetation using high-resolution elevation data. Geophysical Research Letters 26 (16), 2509–2512.

Blair, J., Rabine, D., Hofton, M., 1999. The laser vegetation imaging sensor: A medium-altitude digitisation-only, airborne laser altimeter for mapping vegetation and topography. ISPRS Journal of Photogrammetry & Remote Sensing 54 (2–3), 115–122.

Brenner, A., Zwally, H., Bentley, C., Csathó, B., Harding, D., Hofton, M., Minster, B., Roberts, L., Saba, J., Thomas, R., Yi, D., 2003. Derivation of range and range distributions from laser pulse waveform analysis for surface elevations, roughness, slope, and vegetation heights. Technical Report. Geoscience Laser Altimeter System (GLAS) - Algorithm Theoretical Basis Document Version 4.1. http://www.csr.utexas.edu/glas/pdf/Atbd_20031224.pdf (accessed 24.07.08).

Bretar, F., 2006. Couplage de données laser aéroporté et photogrammétriques pour l'analyse de scènes tridimensionnelles. Ph.D. Thesis. ENST Paris, France.

Carlsson, T., Steinvall, O., Letalick, D., 2001. Signature simulation and signal analysis for 3-D laser radar. Technical Report FOI-R-0163-SE, FOI, Sweden.

Chauve, A., Mallet, C., Bretar, F., Durrieu, S., Pierrot-Deseilligny, M., Puech, W., 2007. Processing full-waveform lidar data: Modelling raw signals. International Archives of Photogrammetry, Remote Sensing and Spatial Information Sciences 36 (Part 3/W52), 102–107.

Chauve, A., Vega, C., Bretar, F., Durrieu, S., Allouis, T., Pierrot-Deseilligny, M., Puech, W., 2008. Processing full-waveform lidar data in an alpine coniferous forest: Assessing terrain and tree height quality. International Journal of Remote Sensing (in press).

Dempster, A., Laird, N., Rubin, D., 1977. Maximum likelihood from incomplete data via the EM algorithm. Journal of the Royal Statistical Society 39 (1), 1–38.

Der, S., Redman, B., Chellapa, R., 1997. Simulation of error in optical radar range measurements. Applied Optics 36 (27), 6869–6874.

Drake, J., Dubayah, R., Clark, D., Knox, R., Blair, J., Hofton, M., Chazdon, R., Weishampel, J., Prince, S., 2002. Estimation of tropical forest structural characteristics using large-footprint lidar. Remote Sensing of Environment 79 (2–3), 305–319.

Dubayah, R., Blair, J., 2000. Lidar remote sensing for forestry applications. Journal of Forestry 98 (6), 44–46.

Ducic, V., Hollaus, M., Ullrich, A., Wagner, W., Melzer, T., 2006. 3D vegetation mapping and classification using full-waveform laser scanning. In: Proc. Workshop on 3D Remote Sensing in Forestry. EARSeL/ISPRS, Vienna, Austria, 14–15 February 2006, pp. 211–217.

Duong, H., Pfeifer, N., Lindenbergh, R., 2006. Full waveform analysis: ICESAT laser data for land cover classification. International Archives of Photogrammetry, Remote Sensing and Spatial Information Sciences 36 (Part 7) (on CD-ROM).

Duong, H., Pfeifer, N., Lindenbergh, R., Vosselman, G., 2008. Single and two epoch analysis of ICESat full-waveform data over forested areas. International Journal of Remote Sensing 29 (5), 1453–1473.

Fidera, A., Chapman, M., Hong, J., 2004. Terrestrial lidar for industrial metrology applications: Modelling, enhancement and reconstruction. International Archives of Photogrammetry, Remote Sensing and Spatial Information Sciences 35 (Part B5), 880–883.

Filin, S., 2002. Surface clustering from airborne laser scanning data. International Archives of Photogrammetry, Remote Sensing and Spatial Information Sciences 34 (Part 3A), 119–124.

GLAS, 2008. Website of GLAS system associated with ICESAT mission. http://glas.gsfc.nasa.gov/ (accessed 31.01.08).

Green, P., 1995. Reversible jump Markov chain Monte-Carlo computation and Bayesian model determination. Biometrika 82 (4), 711–732.

Geophysical Research Letters, 2005. Special issue on Results From Ice, Cloud, and land Elevation Satellite (ICESat) Mission. Geophysical Research Letters 57 (2-3-4).

Gross, H., Jutzi, B., Thoenessen, U., 2007. Segmentation of tree regions using data of a full-waveform laser. International Archives of Photogrammetry, Remote Sensing and Spatial Information Sciences 36 (Part 3/W49A), 57–62.

Guenther, G., Cunningham, A., Rocque, P.L., Reid, D., 2000. Meeting the accuracy challenge in airborne lidar bathymetry. In: Proc. 20th Workshop on Lidar Remote Sensing of Land and Sea, EARSeL, Dresden, Germany, 16–17 June 2000, (on CD-ROM).

Guenther, G., Mesick, H., 1988. Analysis of airborne lidar bathymetric waveforms. In: Proc. of the 9th Ocean Optics. Orlando, FA, USA, SPIE, 4–6 April 1988, pp. 232–241.

Haala, N., Brenner, C., 1999. Extraction of buildings and trees in urban environments. ISPRS Journal of Photogrammetry & Remote Sensing 54 (2–3), 130–137.

Harding, D., Gesch, D., Carabajal, C., Luthcke, S., 1999. Application of the shuttle laser altimeter in an accuracy assessment of GTOPO30, a global 1-kilometer digital elevation model. International Archives of Photogrammetry, Remote Sensing and Spatial Information Sciences 32 (Part 3/W14), 81–85.

Harding, D., Lefsky, M., Parker, G., 2001. Laser altimeter canopy heigh profiles. Methods and validation for closed-canopy, broadleaf forests. Remote Sensing of Environment 76 (9), 283–297.

Heipke, C., Jacobsen, K., Wegmann, H., 2002. Analysis of the results of the OEEPE test 'Integrated sensor orientation'. Technical Report 43, OEEPE Official Publications.

Hernández-Marín, S., Wallace, A., Gibson, G., 2007. Bayesian analysis of lidar signals with multiple returns. IEEE Transactions on Pattern Analysis and Machine Intelligence 29 (12), 2170–2180.

Höfle, B., Pfeifer, N., 2007. Correction of laser scanning intensity data: Data and model-driven approaches. ISPRS Journal of Photogrammetry & Remote Sensing 62 (6), 1415–1433.

Hofton, M., Minster, J., Blair, J., 2000. Decomposition of laser altimeter waveforms. IEEE Transactions on Geoscience and Remote Sensing 38 (4), 1989–1996.

Holmgren, J., Persson, Å., 2004. Identifying species of individual trees using airborne laser scanner. Remote Sensing of Environment 90 (4), 415–423.

Hug, C., Ullrich, A., Grimm, A., 2004. Litemapper-5600—A waveform-digitizing LIDAR terrain and vegetation mapping system. International Archives of Photogrammetry, Remote Sensing and Spatial Information Sciences 36 (Part 8/W2), 24–29.

Hug, C., Wehr, A., 1997. Detecting and identifying topographic objects in laser altimeter scanning data. International Archives of Photogrammetry and Remote Sensing 32 (Part 3-4/W2), 19–26.

Huising, E., Pereira, L.G., 1998. Errors and accuracy estimates of laser data acquired by various laser scanning systems for topographic applications. ISPRS Journal of Photogrammetry & Remote Sensing 53 (5), 1245–1261.

Hyde, P., Dubayah, R., Peterson, B., Blair, J., Hofton, M., Hunsaker, C., Knox, R., Walker, W., 2005. Mapping forest structure for wildlife habitat analysis using waveform lidar: Validation of montane ecosystems. Remote Sensing of Environment 96 (3–4), 427–437.

Hyyppä, J., Hyyppä, H., Litkey, P., Yu, X., Haggrén, H., Rönnholm, P., Pyysalo, U., Pitkänen, J., Maltamo, M., 2004. Algorithms and methods of airborne laser scanning for forest measurements. International Archives of Photogrammetry, Remote Sensing and Spatial Information Sciences 36 (Part 8/W2), 82–89.

ICESat, 2008. Website of the ICESAT mission with in particular technical information and GLAS system data. http://icesat.gsfc.nasa.gov/ (accessed 24.07.08).
Irish, J., Lillycrop, W., 1999. Scanning laser mapping of the coastal zone: The SHOALS system. ISPRS Journal of Photogrammetry & Remote Sensing 54 (2–3), 123–129.
Jelalian, R., 1992. Laser Radar Systems. Artech House, Boston, London.
Jutzi, B., Neulist, J., Stilla, U., 2005. Sub-pixel edge localization based on laser waveform analysis. International Archives of Photogrammetry, Remote Sensing and Spatial Information Sciences 36 (Part 3/W19), 109–114.
Jutzi, B., Stilla, U., 2003. Laser pulse analysis for reconstruction and classification of urban objects. International Archives of Photogrammetry, Remote Sensing and Spatial Information Sciences 34 (Part 3/W8), 151–156.
Jutzi, B., Stilla, U., 2005a. Measuring and processing the waveform of laser pulses. In: Proc. 7th Optical 3-D Measurement Techniques. FIG/IAG/ISPRS, Vienna, Austria, 3–5 October 2005, pp. 194–203.
Jutzi, B., Stilla, U., 2005b. Waveform processing of laser pulses for reconstruction of surfaces in urban areas. International Archives of Photogrammetry, Remote Sensing and Spatial Information Sciences 36 (Part 8/W27) (on CD-ROM).
Jutzi, B., Stilla, U., 2006. Range determination with waveform recording laser systems using a Wiener filter. ISPRS Journal of Photogrammetry & Remote Sensing 61 (2), 95–107.
Kaasalainen, S., Ahokas, E., Hyyppä, J., Suomalainen, J., 2005a. Study of surface brighteness from backscattered laser intensity: Calibration of laser data. IEEE Geoscience and Remote Sensing Letters 2 (3), 255–259.
Kaasalainen, S., Hyyppä, J., Mielonen, T., 2005b. Laboratory calibration of backscattered intensity for laser scanning land targets. International Archives of Photogrammetry, Remote Sensing and Spatial Information Sciences 36 (Part 3/W19), 13–17.
Kimes, D., Ranson, K., Sun, G., Blair, J., 2006. Predicting lidar measured forest vertical structure from multi-angle spectral data. Remote Sensing of Environment 100 (4), 503–511.
Kirchhof, M., Jutzi, B., Stilla, U., 2008. Iterative processing of laser scanning data by full waveform analysis. ISPRS Journal of Photogrammetry & Remote Sensing 63 (1), 99–114.
Koetz, B., Morsdorf, F., Sun, G., Ranson, K., Itten, K., Allgöwer, B., 2006. Inversion of a lidar waveform model for forest biophysical parameter estimation. IEEE Geoscience and Remote Sensing Letters 3 (1), 49–53.
Kotchenova, S., 2005. New approaches to retrieval and application of lidar-measured vegetation vertical canopy profiles. Ph.D. Thesis. University of Boston, USA.
Lachérade, S., Miesch, C., Briottet, X., LeMen, H., 2005. Spectral variability and bidirectional reflectance behaviour of urban materials at a 20 cm spatial resolution in the visible and near infrared wavelengths. A case study over Toulouse (France). International Journal of Remote Sensing 26 (17), 3859–3866.
Lefsky, M., Cohen, W., Acker, S., Parker, G., Spies, T., Harding, D., 1999a. Lidar remote sensing of the canopy structure and biophysical properties of Douglas-fir western hemlock forests. Remote Sensing of Environment 70 (3), 339–361.
Lefsky, M., Cohen, W., Parker, G., Harding, D., 2002. Lidar remote sensing for ecosystem studies. BioScience 52 (1), 19–30.
Lefsky, M., Harding, D., Cohen, W., Parker, G., Shugart, H., 1999b. Surface lidar remote sensing of basal area and biomass in deciduous forests of eastern Maryland, USA. Remote Sensing of Environment 67 (1), 83–98.
LVIS, 2008. LVIS sensor website. http://lvis.gsfc.nasa.gov/ (accessed 24.07.08).
Mallet, C., Soergel, U., Bretar, F., 2008. Analysis of full-waveform lidar data for an accurate classification of urban areas. International Archives of Photogrammetry, Remote Sensing and Spatial Information Sciences 37 (Part 3A), 85–92.
Marquardt, D., 1969. An algorithm for least-squares estimation of nonlinear parameters. Journal of the Society for Industrial and Applied Mathematics 11 (2), 431–441.
Means, J., Acker, S., Harding, D., Blair, J., Lefsky, M., Cohen, W., Harmon, M., McKee, W., 1999. Use of large-footprint scanning airborne lidar to estimate forest stand characteristics in the western cascades of Oregon. Remote Sensing of Environment 67 (3), 298–308.
Ni-Meister, W., Li, X., Woodcock, C.E., Roujean, J.L., Davis, R., 1997. Transmission of solar radiation in boreal conifer forests: Measurements and models. Journal of Geophysical Research 102 (D24), 29555–29566.
Ni-Meister, W., Jupp, D., Dubayah, R., 2001. Modeling lidar waveforms in heterogeneous and discrete canopies. IEEE Transactions on Geoscience and Remote Sensing 39 (9), 1943–1958.
Persson, Å., Holmgren, J., Söderman, U., 2002. Detecting and measuring individual trees using an airborne laser scanner. Photogrammetric Engineering and Remote Sensing 68 (9), 925–932.
Persson, Å., Söderman, U., Töpel, J., Alhberg, S., 2005. Visualization and analysis of full-waveform airborne laser scanner data. International Archives of Photogrammetry, Remote Sensing and Spatial Information Sciences 36 (Part 3/W19), 103–108.
Peterson, B., Ni-Meister, W., Blair, J., Hofton, M., Hyde, P., Dubayah, R., 2001. Modeling lidar waveforms using a radiative transfer model. International Archives of Photogrammetry, Remote Sensing and Spatial Information Sciences 34 (Part 3/W4), 121–124.
Reitberger, J., Krzystek, P., Stilla, U., 2007. Combining tree segmentation and stem detection using full-waveform lidar data. International Archives of Photogrammetry, Remote Sensing and Spatial Information Sciences 36 (Part 3/W52), 332–337.
Reitberger, J., Krzystek, P., Stilla, U., 2008a. Analysis of full waveform LIDAR data for the classification of deciduous and coniferous trees. International Journal of Remote Sensing 29 (5), 1407–1431.
Reitberger, J., Schnörr, C., Krzystek, P., Stilla, U., 2008b. 3D segmentation of full-waveform lidar data for single tree detection using normalized cutes. International Archives of Photogrammetry, Remote Sensing and Spatial Information Sciences 37 (Part 3A), 77–83.
Reutebuch, S., Andersen, H.-E., McGaughey, R., 2005. LIDAR: An emerging tool for multiple resource inventory. Journal of Forestry 103 (6), 286–292.
Roth, R.B., Thompson, J., 2008. Practical application of multiple-pulse in the air (MPiA) lidar in large area surveys. International Archives of Photogrammetry, Remote Sensing and Spatial Information Sciences 37 (Part 1), 183–188.
Rottensteiner, F., Briese, C., 2002. A new method for building extraction in urban areas from high-resolution lidar data. International Archives of Photogrammetry, Remote Sensing and Spatial Information Sciences 34 (Part 3A), 295–301.
Schenk, T., 2001. Modeling and analysing systematic errors in airborne laser scanners. Technical Report. Departement of Civil and Environmental Engineering and Geodetic Science, The Ohio State University, USA.
Sithole, G., 2005. Segmentation and classification of airborne laser scanner data. Ph.D. Thesis. ITC, University of Delft, The Netherlands.
Sithole, G., Vosselman, G., 2006. Bridge detection in airborne laser scanner data. ISPRS Journal of Photogrammetry & Remote Sensing 61 (1), 33–46.
SLICER, 2008. Website of SLICER and SLA sensors. Technical specifications and data available. http://denali.gsfc.nasa.gov/lapf/ (accessed 24.07.08).
Steinvall, O., 2000. Waveform simulation for 3-D sensing laser radars. Technical Report FOI-R-1530-SE, FOI, Sweden.
Stilla, U., Jutzi, B., 2008. Waveform analysis for small-footprint pulsed laser systems. In: Shan, J., Toth, C.K. (Eds.), Topographic Laser Ranging and Scanning: Principles and Processing. CRC Press, Boca Raton, pp. 215–234.
Stilla, U., Yao, W., Jutzi, B., 2007. Detection of weak laser pulses by full-waveform stacking. International Archives of Photogrammetry, Remote Sensing and Spatial Information Sciences 36 (Part 3/W49A), 25–30.
Sun, G., Ranson, K., 2000. Modeling lidar returns from forest canopies. IEEE Transactions on Geoscience and Remote Sensing 38 (6), 2261–2626.
Thiel, K., Wehr, A., 2004. Performance and capabilities of laser scanners - an overview and measurement principle analysis. International Archives of Photogrammetry, Remote Sensing and Spatial Information Sciences 36 (Part 8/W2), 14–18.
Vandapel, N., Amidi, O., Miller, J., 2004. Toward laser pulse waveform analysis for scene interpretation. In: Proc. International Conference on Robotics and Automotion. IEEE, New Orleans, LA, USA, 26 April-1 May 2004, pp. 950–955.
VCL, 2008. Website of the Vegetation Canopy Lidar mission. Technical specifications, publications and data available. http://www.geog.umd.edu/vcl/ (accessed 18.07.08).
Wagner, W., Hollaus, M., Briese, C., Ducic, V., 2008a. 3D vegetation mapping using small-footprint full-waveform airborne laser scanners. International Journal of Remote Sensing 29 (5), 1433–1452.
Wagner, W., Hyyppä, J., Ullrich, A., Lehner, H., Briese, C., Kaasalainen, S., 2008b. Radiometric calibration of full-waveform small-footprint airborne laser scanners. International Archives of Photogrammetry, Remote Sensing and Spatial Information Sciences 37 (Part 1), 163–168.
Wagner, W., Ullrich, A., Ducic, V., Melzer, T., Studnicka, N., 2006. Gaussian decomposition and calibration of a novel small-footprint full-waveform digitising airborne laser scanner. ISPRS Journal of Photogrammetry & Remote Sensing 60 (2), 100–112.
Wagner, W., Ullrich, A., Melzer, T., Briese, C., Kraus, K., 2004. From single-pulse to full-waveform airborne laser scanners: Potential and practical challenges. International Archives of Photogrammetry, Remote Sensing and Spatial Information Sciences 35 (Part B3), 201–206.
Wong, H., Antoniou, A., 1991. Characterization and decomposition of waveforms for LARSEN 500 airborne system. IEEE Transactions on Geoscience and Remote Sensing 29 (6), 912–921.
Yu, X., Hyyppä, J., Kaartinen, H., Maltamo, M., 2004. Automatic detection of harvested trees and determination of forest growth using airborne laser scanning. Remote Sensing of Environment 90 (4), 451–462.
Zwally, H., Schutz, B., Abdalati, W., Abshire, J., Bentley, C., Brenner, A., Bufton, J., Dezio, J., Hancock, D., Harding, D., Herring, T., Minster, B., Quinn, K., Palm, S., Spinhirne, J., Thomas, R., 2002. ICESat's laser measurements of polar ice, atmosphere, ocean, and land. Journal of Geodynamics 34 (3), 405–445.